PNAS RESEARCH ARTICLE | NEUROSCIENCE

Cerebral blood flow is modulated by astrocytic cAMP elevation independently of IP_3R2-mediated Ca^{2+} signaling in mice

Marta Vittani[a], Rasmus Herlo[a,b], Xiaowen Wang[a], Michala Daniela Bach Christensen[a,c], Camilla Trang Vo[a], Tsuneko Mishima[a], Peter Kusk[a], Ayumu Konno[d,e,1], Hirokazu Hirai[d,e], Takashi Tsuboi[f], Tetsuya Kitaguchi[g], Celia Kjaerby[a], Antonis Asiminas[a], Tatsushi Yokoyama[h], Masayuki Sakamoto[h], Maiken Nedergaard[a,i], and Hajime Hirase[a,i,1]

Affiliations are included on p. 11.

Edited by Jeremy Nathans, Johns Hopkins University School of Medicine, Baltimore, MD; received October 24, 2024; accepted June 2, 2025

Local neural activation drives regional increase of cerebral blood flow (CBF), in a phenomenon known as functional hyperemia. Astrocytes, which enwrap cerebral blood vessels and respond to neuronal activity through their G protein–coupled receptors (GPCRs), play a vital role in brain energy metabolism. Although astrocytic calcium (Ca^{2+}) signaling has been widely studied in relation to neurovascular coupling, the role of cyclic adenosine monophosphate (cAMP), another key second messenger of GPCRs, on CBF has not been established. In this study, we explored the effects of optogenetically induced astrocytic cAMP elevation on CBF. We engineered adeno-associated viral vectors (AAVs) to express a bacterial photoactivated adenylyl cyclase in astrocytes, which triggers an increase in cAMP upon blue light stimulation. Opto-stimulation also elevated astrocytic Ca^{2+}, albeit with a delayed onset under mild stimulation. In vivo imaging of anesthetized and awake wild-type mice through a thinned skull preparation revealed that optogenetically induced astrocytic cAMP elevation led to pronounced arteriole dilation, with a latency of 1.8 s and maximal dilation reached within 10 s in the awake state and slower response under anesthesia. Mild opto-stimulation causing sensory-level cAMP elevations was sufficient to induce arteriole dilation. This effect was preserved in IP_3 receptor type 2-knockout ($IP_3R2^{-/-}$) mice, indicating a mechanism independent of GPCR-induced intracellular Ca^{2+} elevations. These findings highlight astrocytic cAMP as a key modulator of cerebral vasodilation, contributing to our understanding of local CBF regulation. This study opens broad avenues for understanding astrocyte-mediated control of CBF and its implications in neurological diseases characterized by dysregulated blood flow.

astrocytes | neurovascular coupling | optogenetic GPCR | cAMP elevation | blood flow

Significance

This research explores how astrocytes, specialized brain cells, regulate cerebral blood flow (CBF). Astrocytes elevate calcium (Ca^{2+}) and/or cyclic adenosine monophosphate (cAMP) after sensing neuronal activity. Astrocytic Ca^{2+} increases have been implicated in CBF regulation, but recent studies challenged this notion. Using optogenetics, researchers found that elevation of cAMP levels in astrocytes induced blood vessels dilation independently of Ca^{2+} elevations. This finding highlights an astrocyte-dependent mechanism of how the brain regulates CBF, which is important for energy metabolism and could help us understand diseases like dementia or stroke that involve disrupted blood flow.

The vertebrate brain is richly supplied by blood vessels to meet the high and ever fluctuating energy demands of electrically active neurons (1), with somas located 8 to 20 μm away from the nearest capillary (2). It is estimated that maintaining the hyperpolarized resting membrane potential and counterbalancing the ion fluxes by action potentials and synaptic currents represent the predominant portion (>90%) of the brain's energy consumption (3). Functional hyperemia, also known as neurovascular coupling, is a mechanism by which cerebral blood flow (CBF) is increased in areas of high neuronal activity. Its physiological role has traditionally been associated with meeting the increased metabolic demand of neurons. More recently, it has also been linked to maintaining brain temperature, signaling to neurons, driving production and circulation of cerebrospinal fluid, transporting of signaling molecules, and stabilizing vasculature (4). Extracellular potassium (K_e^+) and nitric oxide (NO) produced by neuronal activity have been identified as key factors in dilating arterioles through smooth muscle cell relaxation, thereby inducing functional hyperemia (5, 6).

Astrocytes enwrap cerebral blood vessels with their endfeet and surround synapses by their leaflet fine processes (7). This anatomical organization places astrocytes in a unique position to regulate energy metabolism in the brain. For example, they play a critical role in receiving glucose from the bloodstream and delivering lactate to neurons supporting their spiking activities (8). Astrocytes respond to neuronal activity through receptors for neurotransmitters, which are mostly G protein–coupled receptors (GPCRs) (9). Activation of astrocytic GPCRs, such as alpha1 adrenergic receptors or CB1 cannabinoid receptors, leads to large-amplitude increases of cytosolic Ca^{2+} via the inositol-trisphosphate (IP_3)-dependent (Gq) pathway (10, 11). Astrocytic Ca^{2+} elevations were shown to modulate neurovascular coupling by ligand application or neural fiber stimulation, but this role has been repeatedly questioned (12–15). Moreover, IP_3 receptor type2-knockout ($IP_3R2^{-/-}$)

Author contributions: M.V., A.K., C.K., A.A., M.N., and H. Hirase designed research; M.V., R.H., X.W., M.D.B.C., and C.T.V. performed research; X.W., T.M., A.K., H. Hirai, T.T., T.K., T.Y., and M.S. contributed new reagents/analytic tools; M.V., R.H., and P.K. analyzed data; and M.V., A.A., M.N., and H. Hirase wrote the paper.

The authors declare no competing interest.

This article is a PNAS Direct Submission.

[1]To whom correspondence may be addressed. Email: konnoa@gunma-u.ac.jp or hirase@sund.ku.dk.

This article contains supporting information online at https://www.pnas.org/lookup/suppl/doi:10.1073/pnas.2422069122/-/DCSupplemental.

Published July 1, 2025.

mice, in which astrocytes have diminished somatic Ca^{2+} signals, exhibit normal functional hyperemia (16–18). Recently, astrocyte-specific manipulation of intracellular Ca^{2+} dynamics through chemo- or optogenetics demonstrated only subtle effects of astrocytic Ca^{2+} signaling on local blood flow regulation (19, 20). Apart from Gq-mediated IP_3/Ca^{2+} signaling, cyclic adenosine-monophosphate (cAMP) is a major second messenger downstream of astrocytic Gs-coupled GPCR activation including beta adrenergic receptors, D1 dopamine receptors, and A2 adenosine receptors (21). While the activation of astrocytic Gs-GPCRs activation and subsequent cAMP increases have been studied in relation to synaptic plasticity (22–24) and energy metabolism (25), their impact on the vascular dynamics remains unaddressed.

Recently, we engineered adeno-associated viral vectors (AAVs) that enable fluorescent labeling of blood plasma through systemic injection (26, 27). By combining this approach with the expression of an engineered bacterial photoactivated adenylyl cyclase (bPAC) (28), which elevates intracellular cAMP upon blue light illumination, we aimed to investigate the effect of astrocytic cAMP elevation on cerebral cortical vasodynamics in a minimally invasive manner. Our findings revealed that astrocytic cAMP elevation reliably induces arteriole dilation across brain states—in both anesthetized and awake mice—and across a range of stimulation intensities, including very mild opto-stimulation producing only small cAMP increases. cAMP-induced vascular dilation remained unchanged in $IP_3R2^{-/-}$ mice, indicating a mechanism independent of intracellular Ca^{2+}. Our astrocyte-specific manipulation of cAMP suggests a distinct pathway underscoring a direct role of astrocytes in functional hyperemia. The data may also explain the existing controversies in the field.

Results

Astrocytic cAMP Increase Leads to Arteriole Dilation in Anesthetized Mice. To elevate cAMP levels in astrocytes optogenetically, we used the AAV PHP.eB/mGFAP(ABC1D)-2pabPAC(F198Y), which expresses a one-photon and two-photon-activatable bPAC (28) with a single point mutation to reduce constitutive activity (29) under the control of a GFAP promoter. We employed PHP.eB/mGFAP(ABC1D)-Lck-PinkFlamindo, an AAV expressing the red fluorescent cAMP indicator Pink Flamindo (30) anchored to the intracellular astrocytic membrane by the Lck peptide (31) for improved visualization of cAMP changes in fine processes (Fig. 1*A*). Both AAVs were administered systemically via the retro-orbital route to C57BL/6J mice. Three weeks postinjection, in vivo imaging (*SI Appendix*, Fig. S1*A*) and histology (Fig. 1*K*) confirmed selective expression of bPAC and Pink Flamindo in astrocytes throughout the brain, including the cerebral cortex.

To assess bPAC effect on astrocytic cAMP, we applied blue LED light (continuous pulse of 0.2 s, 1 s, or 3 s; 5 mW, ~4 × 4 mm^2)

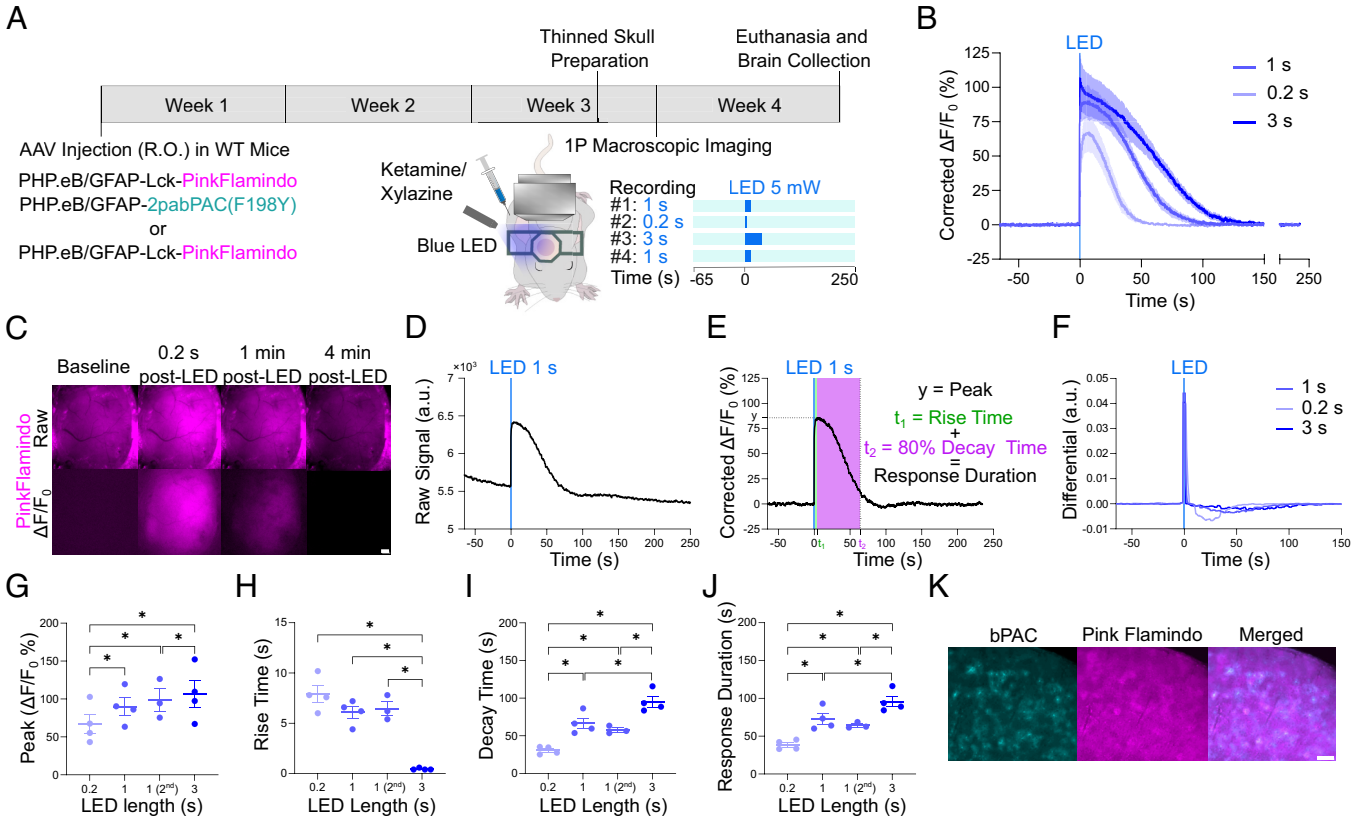

Fig. 1. Opto-stimulation of bPAC induces astrocytic cAMP increase in anesthetized mice. (*A*) Experiment timeline. (*B*) Corrected normalized Pink Flamindo signal following 1-s, 0.2-s, and 3-s bPAC stimulation (n = 4 mice). (*C*) Representative images of raw (*Upper*) and normalized Pink Flamindo fluorescence signal (*Lower*) following 1-s bPAC stimulation. (Scale bar, 500 μm.) (*D*) Representative raw Pink Flamindo fluorescence intensity following 1-s bPAC stimulation. (*E*) A representative trace for background- and photobleaching-corrected normalized Pink Flamindo signal following 1-s bPAC stimulation. Peak is the maximal amplitude. Rise time (highlighted in green) is the time interval for Pink Flamindo to peak, 80% decay time (highlighted in pink) is the time interval for Pink Flamindo to decay to 80% of its peak value and response duration is the sum of rise time and decay time. (*F*) Differentials of Pink Flamindo signal following 1-s, 0.2-s, and 3-s bPAC stimulation (n = 4 mice). (*G–J*) Peak (*G*), rise time (*H*), decay time (*I*), and response duration (*J*) for Pink Flamindo following 1-s (recording #1), 0.2-s, 3-s, and 1-s (recording #4) bPAC stimulation (n = 4 mice for recordings #1–3, 3 mice for #4). Two-sample paired *t* tests followed by correction for false discovery rate (alpha = 0.05) with the Benjamini–Hochberg procedure: *$P < 0.05$. (*K*) Example images of endogenous fluorescence signals from cortical brain slices of mice injected with PHP.eB/mGFAP(ABC1D)-2pabPAC(F198Y) and PHP.eB/mGFAP(ABC1D)-Lck-PinkFlamindo. bPAC and Pink Flamindo are both expressed in astrocytes. (Scale bar, 100 μm.) Graphs plot means ± SEM and individual values.

to the thinned skull over the somatosensory cortex of anesthetized mice, while imaging Pink Flamindo fluorescence (Fig. 1*A*). We observed a dose-dependent increase in fluorescence, reflecting cAMP elevation, in response to bPAC stimulation (Fig. 1 *B* and *C* and *SI Appendix*, Fig. S1 *B–E*). Longer LED stimulation produced higher peak amplitudes and faster rise times, with slower decay to 80% of the peak value (Fig. 1 *G–I* and *SI Appendix*, Table S1). The duration of Pink Flamindo responses also varied with stimulation length (Fig. 1*J* and *SI Appendix*, Table S1). The rate at which fluorescence peaked was similar across different LED stimulation lengths, whereas the return to baseline occurred with varying kinetics (Fig. 1*F*). Of note, 1-s-long stimulation showed similar kinetic profiles at the first and last recordings, demonstrating a strong reproducibility of the stimulation paradigm (Fig. 1*F* and *SI Appendix*, Fig. S1*F*). To further validate bPAC, we systematically injected the AAV into Mlc1-PinkFlamindo transgenic mice expressing the cAMP sensor in astrocytes (*SI Appendix*, Fig. S1*I*). Two-photon microscopy through a cranial window over the somatosensory cortex revealed an increase in Pink Flamindo fluorescence after bPAC activation (*SI Appendix*, Fig. S1 *J* and *K*). Furthermore, physiological cAMP elevations were tested by tail shock-evoked startle response (1.5 to 2 mA, 100 ms) and air puff whisker stimulation (100-ms-long pulses, 5 Hz, 20 psi, duration of 0.5, 1, or 2 min) using one-photon imaging through thinned skull over the somatosensory cortex in wild-type mice expressing Pink Flamindo (*SI Appendix*, Fig. S1*L*). Startle-associated cAMP response was higher and longer in awake compared to anesthetized mice (*SI Appendix*, Fig. S1 *M* and *N*). Following whisker stimulation, cAMP response persisted throughout the stimulation period and its peak amplitude increased proportionally to whisker stimulation length, with 2-min stimulation inducing ~5% increase (*SI Appendix*, Fig. S1 *O* and *P*). These results confirm that optogenetic bPAC stimulation effectively elevates astrocytic cAMP levels in a dose-dependent manner, reaching higher amplitudes and lasting longer than with sensory stimuli.

We next explored whether astrocytic cAMP signaling is causally linked to local CBF. Blood was chronically labeled by coinjecting the bPAC AAV with AAV8/P3-Alb-mScarlet, a liver-targeting AAV expressing albumin (Alb) fused to the red fluorescent protein mScarlet (26) (Alb-mScarlet, Fig. 2*A*). Three weeks later, bPAC expression was observed in cortical astrocytes surrounding superficial vessels labeled by Alb-mScarlet (Fig. 2*C*). To assess the direct effect of bPAC activation on arteriole dilation, we applied blue LED light (0.2 s, 1 s, or 3 s; 5 mW, ~4 × 4 mm^2) to the thinned

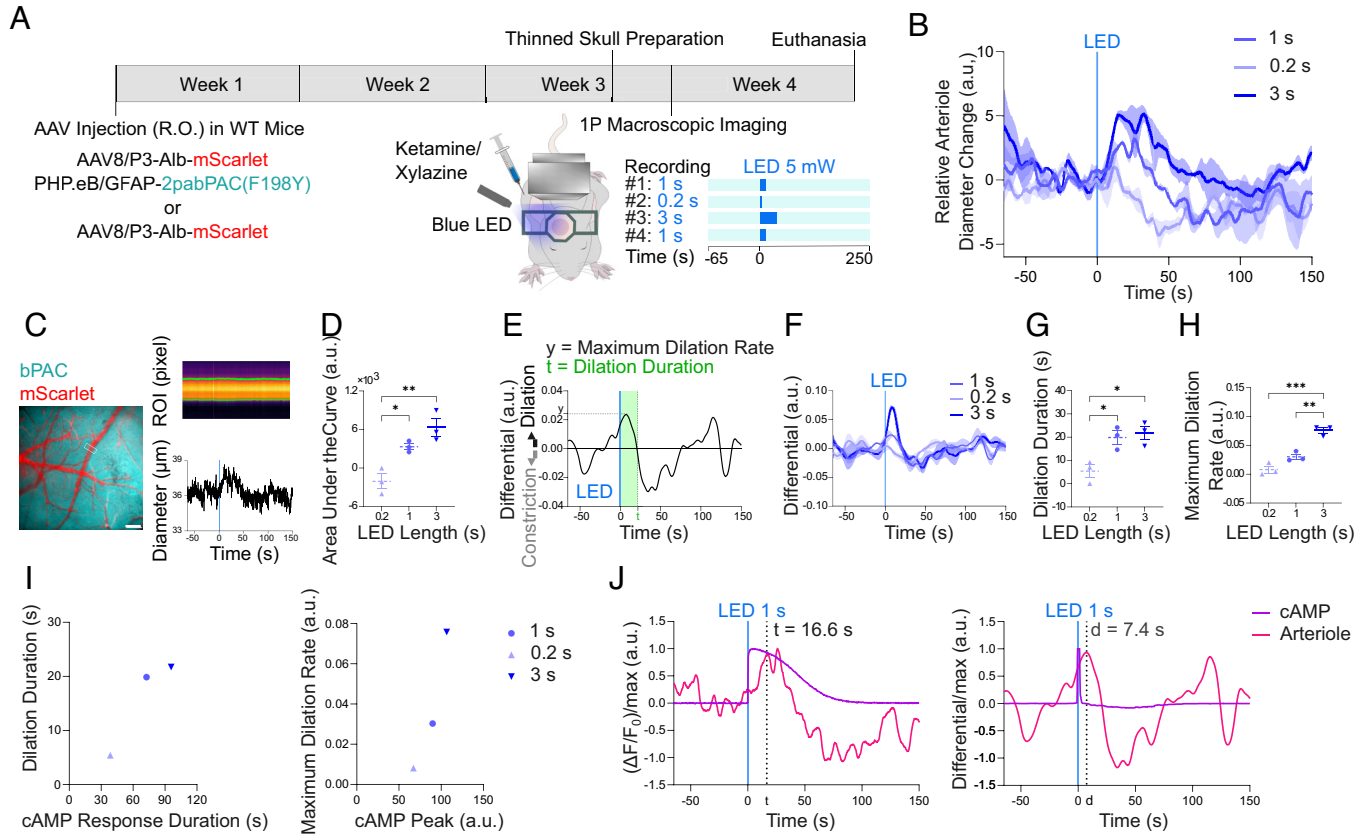

Fig. 2. Opto-stimulation of bPAC induces arteriole dilation in anesthetized mice. (*A*) Experiment timeline. (*B*) Relative arteriole diameter changes following 1-s, 0.2-s, and 3-s bPAC stimulation (n = 3 arterioles from 2 mice; 1-2 arterioles/mouse). (*C*) Representative images of Pink Flamindo and Alb-mScarlet fluorescence signals in astrocytes and vasculature, respectively. A rectangular ROI was defined around the arteriole of interest, and the mean pixel intensity was plotted over time to create a kymograph. The distance between the arteriole borders (highlighted in green in the kymograph) was measured to compute the arteriole diameter changes following 1-s bPAC stimulation. (Scale bar, 100 μm.) (*D*) Area under the curve for the relative arteriole diameter changes measured in the first 38.6 s post-LED stimulation, i.e., half cAMP response duration (n = 3 arterioles from 2 mice; 1-2 arterioles/mouse). One-way ANOVA (F = 0.0041, *P* = 0.0041) followed by post hoc Tukey's multiple comparisons test: **P* < 0.05 and ***P* < 0.01. (*E*) Representative differential of relative arteriole diameter changes following 1-s bPAC stimulation. Positive differential values indicate dilation, whereas negative values indicate constriction. Arteriole dilation duration (highlighted in green) is defined as the time interval where the arteriole dilates for the first time. Maximum dilation rate is the maximal amplitude of this dilation event. (*F–H*) Differentials of relative arteriole diameter changes following 1-s, 0.2-s, and 3-s bPAC stimulation. Arteriole dilation duration (*G*) and maximum dilation rate (*H*) for the differentials measured in the first 38.6 s post-LED stimulation (n = 3 arterioles from 2 mice; 1-2 arterioles/mouse). One-way ANOVA (F = 9.904, *P* = 0.0126 for dilation duration and F = 41.91, *P* = 0.0003 for maximum dilation rate) followed by post hoc Tukey's multiple comparisons test: **P* < 0.05, ***P* < 0.01 and ****P* < 0.001. (*I*) Arteriole dilation duration plotted versus cAMP response duration (*Left*) maximum dilation rate plotted versus cAMP peak (*Right*). (*J*) cAMP response and arteriole dilation following 1-s bPAC stimulation in anesthetized mice (*Left*) and their differentials (*Right*). The black dotted lines indicate the time-to-peak (t) for the arteriole dilation (*Left*) and the delay (d) between cAMP response and arteriole dilation (*Right*). Graphs plot means ± SEM and individual values.

skull above the somatosensory cortex of anesthetized mice while imaging Alb-mScarlet with a fluorescence macroscope (Fig. 2*A*). A dose-dependent biphasic change in arteriole diameter change was observed, starting with an initial dilation followed by a constriction and eventual return to baseline (Fig. 2*B* and *SI Appendix*, Fig. S2 *A–C*). The vasodilator response, measured as the area under the curve in the first 38.6 s post-LED stimulation, corresponding to half of the average Pink Flamindo response duration, increased with 1-s-long and 3-s-long LED stimulation (Fig. 2*D* and *SI Appendix*, Table S2). In contrast, area under the curve decreased for 0.2-s LED stimulation, as the initial dilation lasted for ~15 s only, causing the subsequent constriction to be included in the measurement (Fig. 2*D* and *SI Appendix*, Table S2). This biphasic arteriole diameter response was consistent across all LED stimulations, with spontaneous vasomotion events occasionally observed during the recording (Fig. 2*F*). Longer stimulations resulted in a faster and more prolonged dilation event (Fig. 2 *G* and *H* and *SI Appendix*, Table S2). Based on these findings, we selected the 1-s LED stimulation for subsequent studies, as it was the shortest stimulation that reliably induced significant arteriole dilation. In a larger cohort, 1-s stimulation again produced robust arteriole dilatation in bPAC-expressing mice but not in control mice, confirming previous results (*SI Appendix*, Fig. S2 *E–I* and Table S2). To compare our results with sensory-evoked hyperemia, we successfully triggered arteriole dilation with air puff whisker stimulation (100-ms-long pulses, 5 Hz, 20 psi, duration of 2 min) in the same mice and observed a 2.8% increase in relative arteriole diameter change, comparable to the 3 to 3.6% increase induced by 1-s LED stimulation (*SI Appendix*, Figs. S1*Q* and S2 *A* and *E*).

We found that longer Pink Flamindo responses correspond to more prolonged arteriole dilation (Fig. 2*I* and *SI Appendix*, Fig. S2*J*). Additionally, higher astrocytic cAMP levels lead to faster arteriole dilation (Fig. 2*I* and *SI Appendix*, Fig. S2*J*). The comparison of cAMP profiles with arteriole diameter changes indicated that maximal arteriole dilation occurs after the peak in cAMP increase, with times-to-peak of 12.2 s for 0.2 s stimulation, 16.6 s for 1 s in the first cohort, 13.8 s for 1 s in the second cohort and 15.4 s for 3 s stimulation (Fig. 2*J* and *SI Appendix*, Fig. S2 *D* and *K* and Table S3). Overlaying the cAMP and artery dilation kinetics revealed a consistent delay between astrocytic cAMP elevation and arteriole dilation, with delays of 1.8 s for 0.2 s stimulation, 7.4 s for 1 s in the first cohort, 3.8 s for 1 s in the second cohort and 8.6 s for 3 s stimulation (Fig. 2*J* and *SI Appendix*, Fig. S2 *D* and *K* and Table S3). Together, these findings support our hypothesis that bPAC-induced astrocytic cAMP elevations are causally linked to arteriole dilation in a dose-dependent manner in anesthetized mice.

Astrocytic cAMP Increase Leads to Arteriole Dilation in Awake Mice. Since ketamine and xylazine can affect vascular tone (32) and both cAMP and IP_3-dependent Ca^{2+} signaling in astrocytes (33, 34), we repeated the experiments in awake mice to avoid potential confounding effects from anesthesia. Mice were injected with PHP.eB/mGFAP(ABC1D)-2pabPAC(F198Y) and PHP.eB/mGFAP(ABC1D)-Lck-PinkFlamindo, as before, and the optically induced cAMP elevation response to transcranial LED stimulation was compared to control mice injected only with the Lck-Pink Flamindo AAV (Fig. 3*A*). Similar to anesthetized mice, 1-s LED stimulation significantly increased Pink Flamindo fluorescence in bPAC mice compared to control mice (Fig. 3*B* and *SI Appendix*, Fig. S3 *A–D*). The kinetic profile of cAMP increase was consistent across recordings (*SI Appendix*, Fig. S3*G*), with Pink Flamindo signal peaking at ~3 s, reaching maximal amplitude of ~92.7% and decaying over ~78 s leading to a response duration of ~81 s (Fig. 3 *C* and *D* and *SI Appendix*, Fig. S3 *E* and *F* and Table S1). These findings confirmed that bPAC effectively elevated cAMP levels in astrocytes in awake mice.

Next, we assessed the vasomodulatory effects of astrocytic cAMP dynamics. Awake mice injected with PHP.eB/mGFAP(ABC1D)-2pabPAC(F198Y) and AAV8-P3-Alb-mScarlet were imaged with fluorescence macroscope, together with control mice that received only the blood-labeling AAV (Fig. 3*A*). In bPAC mice, LED stimulation induced a significant arteriole dilation, while control mice showed only a brief and minor dilation, likely due to the blue light exposure (35) (Fig. 3*E* and *SI Appendix*, Fig. S3*H*). Spontaneous vasomotion was occasionally observed. In the first 38.6 s post-LED stimulation, the area under the curve was significantly larger in bPAC mice compared to control (Fig. 3*F* and *SI Appendix*, Table S2). These two groups exhibited distinct differential profiles (Fig. 3*G*). Although the duration of the vasodilatory event was slightly longer in bPAC mice, it was not statistically significant (Fig. 3*H* and *SI Appendix*, Table S2). However, the maximum dilation rate was significantly higher in bPAC compared to control (Fig. 3*I* and *SI Appendix*, Table S2). Overall, the causal bPAC-induced arteriole dilation effect was also observed in awake mice.

The bPAC-induced arteriole dilation in awake mice mirrored the results obtained under anesthesia with 1-s LED stimulation (Fig. 3*J*). Similarly, the correlation between cAMP peak and maximum dilation rate was comparable between awake and anesthetized mice (Fig. 3*J*). In awake mice, astrocytic cAMP elevation induced arteriole dilation with a delay of 1.8 s, with the dilation occurring as the cAMP increase began to decelerate and peaking at 9 s (Fig. 3*K* and *SI Appendix*, Table S3). These results demonstrated the reproducibility of the bPAC-induced vasodilatory effect in awake mice.

cAMP-Induced Arteriole Dilation Is Independent from Large Astrocytic Ca^{2+} Signals. To determine whether the cAMP-induced arteriole dilation depends on astrocytic Ca^{2+} signaling, we repeated the experiments in the $IP_3R2^{-/-}$ mouse model (36), where large IP_3-dependent cytosolic Ca^{2+} elevations are diminished (37, 38). Mice were imaged in the awake state to avoid potential confounding effects from anesthesia on Ca^{2+} and cAMP signaling (33, 34).

In the cAMP study, 1-s- LED stimulation of bPAC successfully induced astrocytic cAMP elevations in both $IP_3R2^{-/-}$ and $IP_3R2^{+/+}$ mice (Fig. 4*A* and *SI Appendix*, Fig. S3 *I–K*). The kinetic profiles were consistent between groups and highly reproducible within each group (*SI Appendix*, Fig. S3 *L–N*). In $IP_3R2^{-/-}$ mice, Pink Flamindo signal peaked at 7.2 s, reaching a maximum of 62.2%, and decayed over 62.3 s, with a total response duration of 69.5 s (Fig. 4 *B–E* and *SI Appendix*, Table S1). Similarly, in $IP_3R2^{+/+}$ mice, Pink Flamindo signal peaked at 8.4 s, reaching a maximum of 54.4%, and decayed to baseline over 76.7 s, with a total response duration of 85.1 s (Fig. 4 *B–E* and *SI Appendix*, Table S1). There was no statistically significant difference between the two groups (Fig. 4 *B–E*). These results suggest that the bPAC-induced cAMP increase in astrocytes is independent of large cytosolic Ca^{2+} increases.

In the vasodilatation study, 1-s LED stimulation of bPAC induced similar arteriole diameter changes in both $IP_3R2^{-/-}$ and $IP_3R2^{+/+}$ mice, with comparable differential profiles (Fig. 4*F* and *SI Appendix*, Fig. S3*O*). The area under the curve in the first 38.6 s post-LED stimulation was not significantly different between the two groups (Fig. 4*G* and *SI Appendix*, Table S2). The duration of the first arteriole dilation event and maximum dilation rate were also similar (Fig. 4 *H* and *I* and *SI Appendix*, Table S2). These findings indicate that the bPAC-induced arteriole dilation effect is preserved in both awake $IP_3R2^{-/-}$ and $IP_3R2^{+/+}$ mice, suggesting

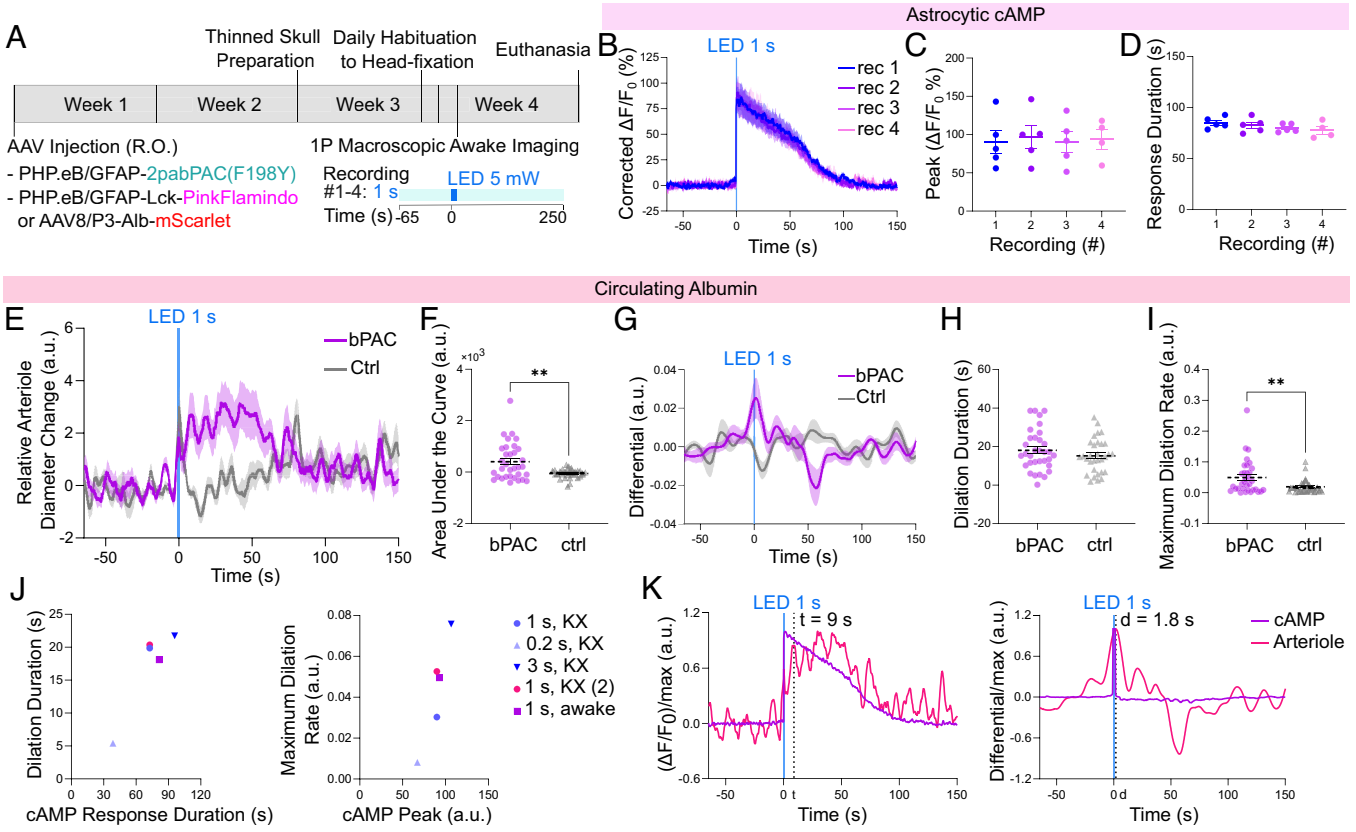

Fig. 3. Opto-stimulation of bPAC induces astrocytic cAMP increase and arteriole dilation in awake mice. (*A*) Experiment timeline. (*B–D*) cAMP imaging. Corrected normalized Pink Flamindo signal (*B*), peak (*C*), and response duration (*D*) following 1-s bPAC stimulation in awake WT mice (n = 5 mice). Mixed-effects analysis using a REML model: $F_{1.823,\,6.685} = 0.7991$, $P = 0.4775$ for peak (*C*); $F_{0.6271,\,2.299} = 3.251$, $P = 0.1797$ for response duration (*D*). (*E–I*) Arteriole imaging. Relative arteriole diameter changes (*E*) following 1-s bPAC stimulation in bPAC and control WT mice. Area under the curve (*F*) measured in the first 38.6 s post-LED stimulation, i.e., half cAMP response duration. Differentials of relative arteriole diameter changes (*G*). Arteriole dilation duration (*H*) and maximum dilation rate (*I*) for the differentials measured in the first 38.6 s post-LED stimulation. N = 33 arterioles from 5 bPAC mice and 31 arterioles from 5 ctrl mice; 5 to 8 arterioles/mouse. Unpaired *t* test: t = 3.445, df = 62, $^{**}P < 0.01$ (*F*), t = 1.171, df = 62, $P = 0.2462$ (*H*); t = 2.754, df = 62, $^{**}P < 0.01$ (*I*). (*J*) Arteriole dilation duration plotted versus cAMP response duration (*Left*) and maximum dilation rate plotted versus cAMP peak (*Right*). (*K*) cAMP response and arteriole dilation following 1-s bPAC stimulation in awake mice (*Left*) and their differentials (*Right*). The black dotted lines indicate the time-to-peak (t) for the arteriole dilation (*Left*) and the delay (d) between cAMP response and arteriole dilation (*Right*). Graphs plot means ± SEM and individual values.

relatively minimal involvement of the astrocytic IP_3/Ca^{2+} signaling in this process.

When correlating cAMP response duration with arteriole dilation, the IP_3R2 mice showed similar response to awake and anesthetized WT mice (Fig. 4*J*). Both cAMP peaks and maximum dilation rate were slightly lower in $IP_3R2^{-/-}$ and $IP_3R2^{+/+}$ mice compared to WT (Fig. 4*J*). Astrocytic cAMP elevations induced arteriole dilation with a delay of 2.8 s in $IP_3R2^{-/-}$ mice and 9.4 s in $IP_3R2^{+/+}$ mice, with arteriole dilation peaking at 22.4 s and 23.6 s, respectively (Fig. 4*K* and *SI Appendix*, Table S3). Overall, these results demonstrate that astrocytic cAMP elevations can induce arteriole dilation independent of the IP_3/Ca^{2+} pathway.

bPAC Opto-Stimulation Induces Astrocytic Ca^{2+} Increase. To assess the effect of bPAC activation on astrocytic Ca^{2+}, we coinjected PHP.eB/mGFAP(ABC1D)-2pabPAC(F198Y) with PHP.eB/hGFAP(ABC1D)-RCaMP3, an AAV expressing the red fluorescent Ca^{2+} indicator RCaMP3 (39) (Fig. 5*A*). Histology confirmed selective expression of bPAC and RCaMP3 in astrocytes (*SI Appendix*, Fig. S4*AA*).

When blue LED light of varying lengths (0.2 s, 1 s, or 3 s; 5 mW) was applied on the somatosensory cortex via the thinned skull in anesthetized mice, RCaMP3 signals increased following bPAC activation (Fig. 5*B* and *SI Appendix*, Fig. S4 *A–D*). Peak amplitudes decreased with subsequent recordings (Fig. 5*C* and *SI Appendix*, Table S4), likely reflecting depletion of intracellular Ca^{2+} stores. Shorter LED stimulation resulted in faster rise times (*SI Appendix*, Fig. S4*F* and Table S4). The first and fourth 1-s recordings showed decay times and durations similar to 3-s and 0.2-s stimulations, respectively (Fig. 5*D* and *SI Appendix*, Fig. S4*G* and Table S4). RCaMP3 signals peaked at similar rates across different LED stimulation lengths, but baseline return varied (*SI Appendix*, Fig. S4*E*).

As in anesthetized mice, 1-s LED stimulation significantly elevated RCaMP3 signals in awake bPAC mice (Fig. 5*E* and *SI Appendix*, Fig. S4 *K–N*). While peak amplitudes declined across recordings, the kinetic profiles remained consistent, with RCaMP3 signal peaking at ~ 2 s and decaying over ~38 s leading to a response duration of ~40 s (Fig. 5 *F* and *G* and *SI Appendix*, Fig. S4 *O–Q* and Table S4). These findings demonstrate that astrocytic bPAC activation elevates intracellular Ca^{2+} of WT mice across different states.

The bPAC-induced Ca^{2+} elevation was markedly reduced in $IP_3R2^{-/-}$ compared to $IP_3R2^{+/+}$ mice (Fig. 5*H* and *SI Appendix*, Fig. S4 *R–T*), mirroring the reduction seen in startle-evoked responses (*SI Appendix*, Fig. S4*Z*). Kinetic profiles varied between groups but were highly consistent within each group (*SI Appendix*, Fig. S5 *W–Y*). As before, each group showed reduced peak amplitudes in successive recordings (Fig. 5*I* and *SI Appendix*, Table S4). In $IP_3R2^{+/+}$ mice, RCaMP3 signals peaked at 1.8 s and decayed to baseline over 20.4 s, with a total response duration of 22.2 s (Fig. 5*J* and *SI Appendix*, Fig. S4 *U* and *V* and Table S4).

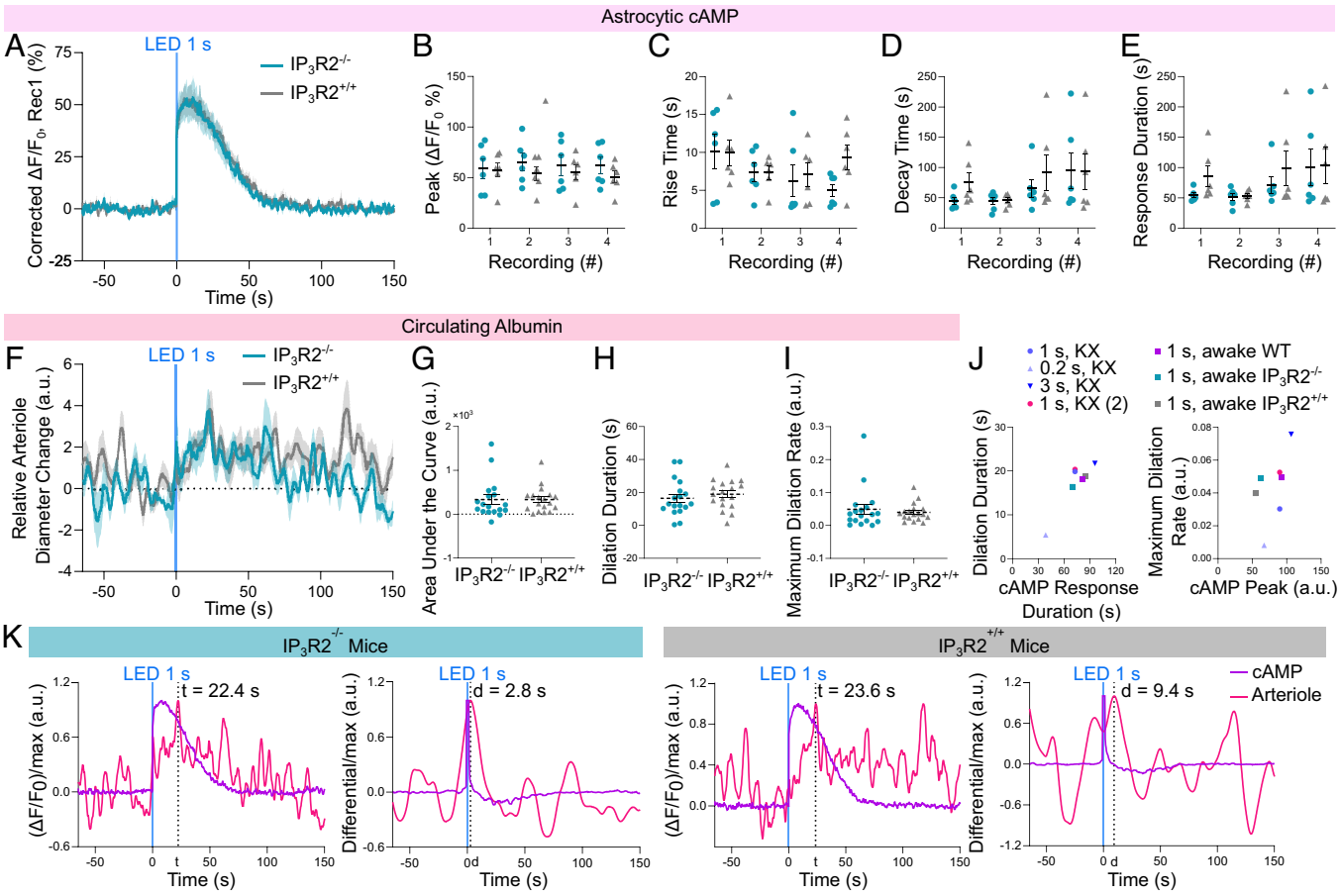

Fig. 4. bPAC-induced arteriole dilation is independent from large astrocytic Ca^{2+} signals. (*A–E*) cAMP imaging. Corrected normalized Pink Flamindo signal (*A*), peak (*B*) rise time (*C*), decay time (*D*), and response duration (*E*) following 1-s bPAC stimulation in awake $IP_3R2^{-/-}$ and $IP_3R2^{+/+}$ mice (n = 6 mice per group). Two-way ANOVA for peak (*B*): $F_{1,\ 10} = 0.5064$, $P = 0.4930$ for genotype; $F_{2.640,\ 26.40} = 0.5748$, $P = 0.6156$ for recording; $F_{3,\ 30} = 1.626$, $P = 0.2042$ for genotype × recording. Two-way ANOVA for rise time (*C*): $F_{1,\ 10} = 0.6943$, $P = 0.4242$ for genotype; $F_{1.996,\ 19.96} = 2.297$, $P = 0.1266$ for recording; $F_{3,\ 30} = 1.143$, $P = 0.3478$ for genotype × recording. Two-way ANOVA for decay time (*D*): $F_{1,\ 10} = 0.9511$, $P = 0.3524$ for genotype; $F_{1.622,\ 16.22} = 2.411$, $P = 0.1285$ for recording; $F_{3,\ 30} = 0.3636$, $P = 0.7797$ for genotype × recording. Two-way ANOVA for response duration (*E*): $F_{1,\ 10} = 1.139$, $P = 0.3109$ for genotype; $F_{1.620,\ 16.20} = 2.262$, $P = 0.1427$ for recording; $F_{3,\ 30} = 0.3115$, $P = 0.8169$ for genotype × recording. (*F–I*) Arteriole imaging. Relative arteriole diameter changes (*F*) following 1-s bPAC stimulation in $IP_3R2^{-/-}$ and $IP_3R2^{+/+}$ mice. Area under the curve (*G*) measured in the first 38.6 s post-LED stimulation. Arteriole dilation duration (*H*) and maximum dilation rate (*I*) for the differentials measured in the first 38.6 s post-LED stimulation. N = 41 arterioles from 6 $IP_3R2^{-/-}$ mice, 34 arterioles from 5 $IP_3R2^{+/+}$ mice; 5 to 8 arterioles/mouse. Unpaired *t* test: t = 0.0048, df = 34, $P = 0.9962$ (*G*), t = 0.7425, df = 34, $P = 0.4629$ (*H*); t = 0.5705, df = 34, $P = 0.5721$ (*I*). (*J*) Arteriole dilation duration plotted versus cAMP response duration (*Left*) and maximum dilation rate plotted versus cAMP peak (*Right*). (*K*) For both $IP_3R2^{-/-}$ (green header) and $IP_3R2^{+/+}$ mice (gray header), cAMP response and arteriole dilation following 1-s bPAC stimulation (*Left*) and their differentials (*Right*). The black dotted lines indicate the time-to-peak (t) for the arteriole dilation (*Left*) and the delay (d) between cAMP response and arteriole dilation (*Right*). Graphs plot means ± SEM and individual values.

Conversely, in $IP_3R2^{-/-}$ mice, RCaMP3 signal peaked at 2.4 s and decayed over 5.4 s, with a total response duration of 7.8 s (Fig. 5*J* and *SI Appendix*, Fig. S4 *U* and *V* and Table S4). These results show that $IP_3R2^{-/-}$ exhibited significantly smaller and slightly delayed Ca^{2+} elevations following bPAC stimulation compared to $IP_3R2^{+/+}$ mice.

The Ca^{2+} increase observed in bPAC mice began concurrently with cAMP elevation, sharply declined before the onset of arteriole dilation and further decreased throughout the dilation period, suggesting it may be a downstream effect of cAMP signaling rather than a driver of sustained hyperemia (*SI Appendix*, Fig. S5 *A–D*). This occurred with LED stimulations of varying lengths (*SI Appendix*, Fig. S4 *H–J*), in different brain states (*SI Appendix*, Figs. S4*J* and S5 *A* and *B*) and in both WT and IP_3R2 mice (*SI Appendix*, Figs. S4*J* and S5 *A–D*). Two-photon imaging of simultaneous cAMP and Ca^{2+} dynamics revealed that bPAC activation induces a transient Ca^{2+} elevation and a sustained increase in cAMP levels (*SI Appendix*, Fig. S5 *E–H*). Consistent with the one-photon experiments, the temporal profile of the cAMP response aligns well with prolonged arteriole expansion (*SI Appendix*, Fig. S5 *A–D* and *H*). Of note, the magnitude of the Ca^{2+} transient was positively correlated with the peak cAMP level, suggesting a graded Ca^{2+} response by cAMP magnitude (*SI Appendix*, Fig. S5*I*). Overall, these results provide evidence for the involvement of IP_3R2 in Ca^{2+} elevation observed following bPAC-induced cAMP increase but suggest weaker coupling to vasodilation compared to cAMP profiles.

Mild bPAC Activation Increases Astrocytic cAMP and Ca^{2+} to Promote Arteriole Dilation. To assess the effect of smaller cAMP elevations, we shortened the LED stimulation to 25 ms and reduced LED intensity from 5 mW to 1 mW. We then applied this mild opto-stimulation to anesthetized mice expressing bPAC and Lck-PinkFlamindo or RCaMP3 in astrocytes, or Alb-mScarlet in blood (Fig. 6*A*).

In the cAMP study, 25-ms LED stimulation significantly increased Pink Flamindo fluorescence (Fig. 6*C*). The Pink Flamindo signal peaked at ~6 s, reaching maximal amplitude of ~8% and decaying over ~22 s leading to a response duration of ~28 s (Fig. 6 *D* and *E* and *SI Appendix*, Fig. S6 *A* and *B* and Table S1). Interestingly, this cAMP response was similar in peak amplitude and kinetics to cAMP elevations triggered by whisker

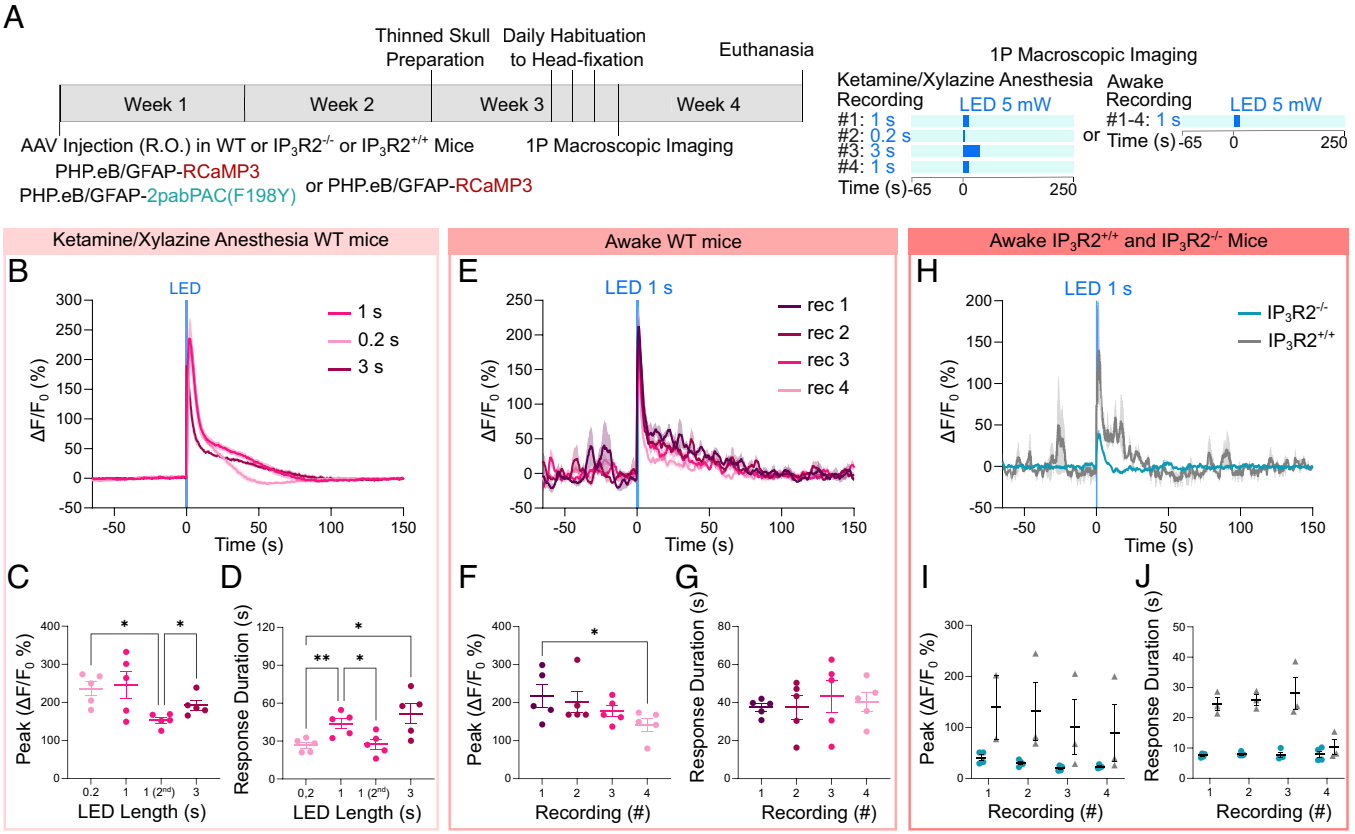

Fig. 5. bPAC opto-stimulation induces astrocytic Ca^{2+} increase. (*A*) Experiment timeline. (*B–D*) Imaging in ketamine–xylazine anesthetized WT mice. Normalized RCaMP3 signal (*B*), peak (*C*), and response duration (*D*) following 1-s, 0.2-s, and 3-s bPAC stimulation (n = 5 mice). Repeated measures one-way ANOVA for recording: $F_{1.464, 5.857} = 7.181$, $P = 0.0311$ for peak (*C*); $F_{1.327, 5.307} = 13.51$, $P = 0.0108$ for response duration (*D*). (*E–G*) Imaging in awake habituated WT mice. Normalized RCaMP3 signal (*E*), peak (*F*), and response duration (*G*) following 1-s bPAC stimulation (n = 5 mice). Repeated measures one-way ANOVA for recording: $F_{1.843, 7.373} = 5.083$, $P = 0.0428$ for peak (*F*); $F_{1.702, 6.810} = 2.069$, $P = 0.1989$ for response duration (*G*). (*H–J*) Imaging in awake habituated $IP_3R2^{-/-}$ and $IP_3R2^{+/+}$ mice. Normalized RCaMP3 signal (*H*), peak (*I*), and response duration (*J*) following 1-s bPAC stimulation (n = 4 $IP_3R2^{-/-}$ and 3 $IP_3R2^{+/+}$ mice). Mixed-effects analysis using a REML model for peak (*I*): $F_{1, 3} = 4.477$, $P = 0.1247$ for genotype; $F_{3, 9} = 13.37$, $P = 0.0012$ for recording; $F_{3, 4} = 6.162$, $P = 0.0557$ for genotype × recording. Two-way ANOVA for response duration (*J*): $F_{1, 5} = 324.4$, $P < 0.0001$ for genotype; $F_{1.563, 7.815} = 6.509$, $P = 0.0259$ for recording; $F_{3, 15} = 6.856$, $P = 0.0040$ for genotype × recording. Graphs plot means ± SEM and individual values.

stimulation and tail shock (*SI Appendix*, Fig. S1 *M–P*). These findings confirmed that reduced bPAC stimulation can effectively elevate cAMP in astrocytes to levels comparable to those induced by sensory stimulation.

In the Ca^{2+} study, RCaMP3 fluorescence increased following 25-ms LED stimulation in bPAC mice, whereas such Ca^{2+} elevation was absent in control mice (Fig. 6*F* and *SI Appendix*, Fig. S6 *E–H*). RCaMP3 signal peaked at ~8.5 s, reaching maximal amplitude of ~73% and decaying over ~8.5 s leading to a response duration of ~17 s (Fig. 6 *G* and *H* and *SI Appendix*, Fig. S6 *C* and *D* and Table S4). These data show that even the low-intensity, brief bPAC activation can elevate astrocytic Ca^{2+} levels.

In the vasodilatation study, 25-ms LED stimulation induced a significant arteriole dilation compared to controls (Fig. 6*I*). The area under the curve during the first 14 s after LED stimulation, corresponding to half of the average Pink Flamindo response duration, was significantly increased in bPAC compared to control mice (Fig. 6*J*). Although dilation duration and maximum dilation rate were slightly higher in bPAC mice, it was not statistically significant (Fig. 6 *K* and *L* and *SI Appendix*, Table S2). Overall, even the minimal bPAC stimulation is sufficient to induce arteriole dilation.

Arteriole dilation occurred 1.2 s after LED stimulation, coinciding with the onset of cAMP elevation, which peaked 6.2 s after stimulation (Fig. 6*B*). Astrocytic Ca^{2+} increased only after cAMP elevation, peaking 7.6 s after stimulation (Fig. 6*B*). In summary, this dataset demonstrates that mild bPAC stimulation, comparable to physiological settings, elevates astrocytic cAMP leading to arteriole dilation and astrocytic Ca^{2+} increase.

Discussion

Given their close association with both vasculature and synapses, astrocytes are ideally positioned to modulate functional hyperemia. While much of the research over the last two decades has focused on the astrocytic second messenger Ca^{2+} (12), this study examines astrocytic cAMP signaling in relation to CBF. To explore the correlative and causal relationship between astrocytic cAMP and vessel dynamics, we selectively expressed an optogenetic cAMP actuator and a cAMP biosensor in astrocytes, while labeling blood plasma with Alb-mScarlet through systemic AAV administration. Additionally, we used a thinned skull preparation to minimize inflammation and reactive gliosis (40). This approach allowed us to investigate the effect of astrocytic cAMP elevations on CBF using minimally invasive optical imaging. We found that 1-s bPAC activation in cerebral cortical astrocytes reliably elevated cAMP levels for over than 1 min and triggered vasodilation in surface arterioles within 2 to 8 s, peaking at 10 to 15 s, in both awake and anesthetized mice. Similarly, milder bPAC activation caused a 28-s elevation in cAMP levels, accompanied by arteriole dilation in anesthetized mice. Using an AAV-encoded Ca^{2+} biosensor, we also observed that bPAC stimulation induces astrocytic Ca^{2+} elevations and milder activation revealed how these are

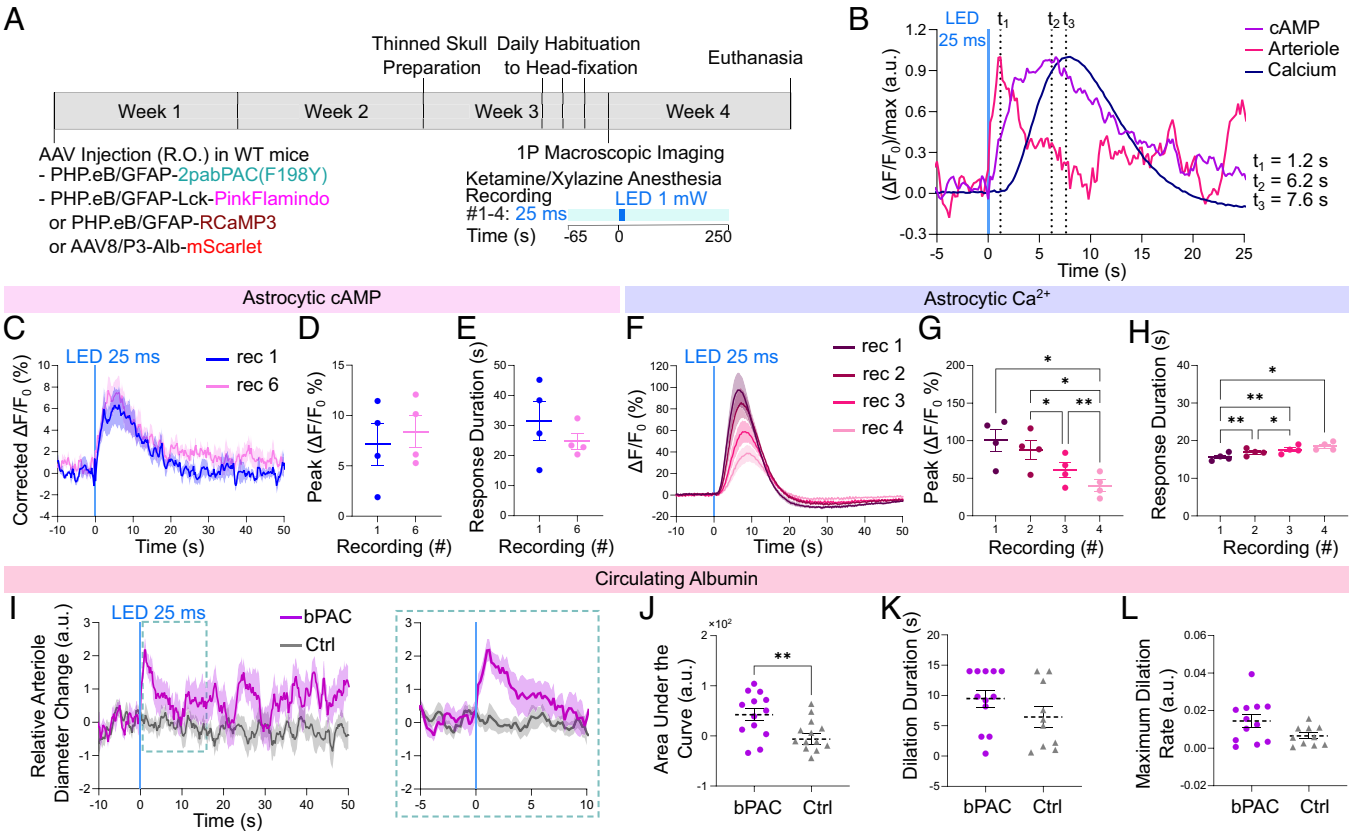

Fig. 6. Mild bPAC activation increases astrocytic cAMP and Ca^{2+} to promote arteriole dilation. (*A*) Experiment timeline. (*B*) Calcium response, cAMP response, and arteriole dilation following 25-ms bPAC stimulation in anesthetized mice. The black dotted lines indicate the time-to-peak for cAMP response (t_2), calcium response (t_3), and arteriole dilation (t_1) from stimulation onset. (*C–E*) cAMP imaging. Corrected normalized Pink Flamindo signal (*C*), peak (*D*), and response duration (*E*) following 25-ms bPAC stimulation (n = 4 mice). Paired *t* test: t = 1.141, df = 3, *P* = 0.3368 (*D*); t = 1.214, df = 3, *P* = 0.3117 (*E*). (*F–H*) Ca^{2+} imaging. Normalized RCaMP3 signal (*F*), peak (*G*), and response duration (*H*) following 25-ms bPAC stimulation (n = 4 mice). Repeated measures one-way ANOVA for recording: $F_{1.188, 3.563} = 29.66$, *P* = 0.0072 for peak (*G*); $F_{1.193, 3.580} = 41.22$, *P* = 0.0041 for response duration (*H*). (*I–L*) Arteriole imaging. Relative arteriole diameter changes (*I*) following 25-ms bPAC stimulation, with zoomed-in area used for quantification. Area under the curve (*J*) measured in the first 14 s post-LED stimulation. Arteriole dilation duration (*K*) and maximum dilation rate (*L*) for the differentials measured in the first 14 s post-LED stimulation. N = 13 arterioles from 6 bPAC mice and 14 arterioles from 4 ctrl mice (*I* and *J*) or 12 arterioles from 5 bPAC mice and 10 arterioles from 4 ctrl mice (*K* and *L*); 1 to 5 arterioles/mouse. Unpaired *t* test: t = 2.925, df = 25, $^{**}P < 0.01$ (*J*); t = 1.389, df = 20, *P* = 0.1802 (*K*); t = 2.045, df = 20, *P* = 0.0543 (*L*). Graphs plot means ± SEM and individual values.

secondary to cAMP increase. Remarkably, astrocytic cAMP-induced hyperemia occurred in $IP_3R2^{-/-}$ mice, suggesting that the process is independent of large cytosolic Ca^{2+} surges. These findings suggest a causal role for astrocytic cAMP in modulating brain vasodilation.

In our study, anesthesia was induced by a single i.p. injection of ketamine (70 mg/kg) and xylazine (10 mg/kg). This anesthetic cocktail is known to generally suppress astrocytic Ca^{2+} transients (33). Regarding astrocytic cAMP, ketamine anesthesia has been suggested to elevate astrocytic cAMP levels (34), whereas xylazine inhibits adenylyl cyclase via activation of alpha-2 adrenergic receptors (41). Given that astrocytes express alpha-2a adrenergic receptors (42), it is plausible that xylazine has a suppressive effect on cAMP dynamics. Indeed, although 1-s bPAC stimulation induced similar cAMP increases in anesthetized and awake mice, a faster rise time and a slower decay were observed in awake mice (Figs. 1 *G–J* and 3 *C* and *D* and *SI Appendix*, Fig. S3 *E* and *F* and Table S1). These differences likely reflect the combined effect of ketamine and xylazine on cAMP signaling. Nevertheless, the robust vasodilatory response to astrocytic cAMP elevation was consistent in both anesthetized and awake mice (Figs. 2 *D*, *G*, and *H* and 3 *F*, *H*, and *I* and *SI Appendix*, Fig. S2 *F*, *H*, and *I* and Table S2), suggesting that the threshold cAMP concentration required to induce arteriole dilation was achieved under both conditions. Additionally, smaller, bPAC-independent arteriole dilation events, representing spontaneous physiological vasomotion (43), were occasionally observed during awake recordings and less frequently under anesthesia. It is noteworthy that a previous study has shown that blue light alone can induce vasodilation in ketamine–xylazine anesthetized mice (35). In our experiment, a small vasodilatory effect was observed in awake control mice expressing only Alb-mScarlet (*SI Appendix*, Fig. S3*H*), but not in anesthetized mice (*SI Appendix*, Fig. S2 *A–C* and *E*). This effect may be due to activating visual pathways by optogenetic stimulation, which could influence broader cortical areas.

Functional hyperemia occurs within ~1 to 2 s after sensory stimulation (44) and is affected by anesthesia (45, 46). Accordingly, we observed that hyperemia following 1-s bPAC activation was faster in awake than anesthetized mice, with arteriole dilation occurring in 1.8 s and peaking at 9 s (Figs. 2*J* and 3*K* and *SI Appendix*, Fig. S2*K* and Table S3). Notably, the delay and time-to-peak of the arteriole dilation response to the cAMP increase depended on bPAC stimulation length in anesthetized mice (Fig. 2*J* and *SI Appendix*, Fig. S2 *D* and *K* and Table S3). With milder bPAC stimulation in anesthetized mice, arteriole dilation peaked 1.2 s after stimulation, coinciding with Pink Flamindo (cAMP) response onset (Fig. 6*B*). Pink Flamindo signal peaked 5 s after maximal arteriole dilation, conceivably due to the sensor's low affinity, which resulted in a delayed indication of small cAMP increases (Fig. 6*B*). The shorter time-to-peak observed for arteriole dilation following milder bPAC stimulation (Fig. 6*B*), compared to stronger 1-s and 3-s stimulations (Fig. 2*J* and

SI Appendix, Fig. S2 *D* and *K*), is likely attributable to the smaller magnitude of the response (Figs. 2*B* and 6*I* and *SI Appendix*, Fig. S2*E*). Specifically, the maximal relative diameter change was 2.2% with mild bPAC activation versus 3 to 5% with stronger stimulation, making it reasonable that a larger dilation requires additional time to reach its peak response (Figs. 2*B* and 6*I* and *SI Appendix*, Fig. S2*E*).

In our study, we found that bPAC stimulation also induced astrocytic Ca^{2+} elevation (Figs. 5 and 6 *F*–*H*). The main source of this Ca^{2+} is likely the endoplasmic reticulum (ER) rather than the extracellular space, since Ca^{2+} elevation is largely attenuated in $IP_3R2^{-/-}$ mice, while the residual Ca^{2+} could come from other sources (47–49). Progressive signal decreases that occurred with the repeated stimulation further supports depletion of this intracellular Ca^{2+} reservoir (Figs. 5 *C*, *F*, and *I* and 6*G*). While 1-s bPAC stimulation induced apparently simultaneous elevations of astrocytic cAMP and Ca^{2+} (*SI Appendix*, Figs. S4*J* and S5 *A* and *B*), mild bPAC activation revealed a delayed Ca^{2+} response by a few seconds relative to cAMP (Fig. 6*B*). The Ca^{2+} response following tail shock or 1-s bPAC stimulation was reduced, but not completely absent, in $IP_3R2^{-/-}$ mice compared to $IP_3R2^{+/+}$ mice (Fig. 5*H* and *SI Appendix*, Fig. S4 *R*–*T* and *Z*). Accordingly, $IP_3R2^{-/-}$ mice showed residual Ca^{2+} response during running (48). Even without IP_3R2, Ca^{2+} can still be released from the ER via the less abundantly expressed isoforms IP_3R1 and IP_3R3 (49), or via ryanodine receptors (47). Alternatively, extracellular Ca^{2+} influx can occur via plasma membrane Ca^{2+} channels, either via NMDA or P2X receptors or via store-operated calcium entry (47). In 5mW LED experiments, bPAC triggered cAMP and Ca^{2+} increases rapidly, both preceding arteriole dilation; however, whereas Ca^{2+} returned to baseline relatively quickly, cAMP remained elevated throughout the entire dilation period, correlating well with the vascular dynamics (*SI Appendix*, Fig. S5 *A*–*D*). Two-photon imaging of GCaMP6f and Pink Flamindo confirmed these temporal profiles, with cAMP response starting slightly after Ca^{2+} most probably due to Pink Flamindo's low affinity and revealed a correlated Ca^{2+} response magnitude with cAMP elevation magnitude (*SI Appendix*, Fig. S5 *E*–*I*). Importantly, with mild bPAC activation, Ca^{2+} increase occurred after arteriole dilation and cAMP increase (Fig. 6*B*). Thus, bPAC-induced Ca^{2+} increase, while downstream of cAMP signaling, is unlikely to play a causal role in this type of hyperemia.

Awake $IP_3R2^{-/-}$ mice exhibited cAMP dynamics similar to those of $IP_3R2^{+/+}$ mice (Figs. 3 *C* and *D* and 4 *B*–*E* and *SI Appendix*, Fig. S3 *E* and *F* and Table S1), indicating that the absence of large cytosolic Ca^{2+} surges in astrocytes has minimal impact on bPAC-induced cAMP elevation. Consistently, we observed that arterioles dilate to the same extent in $IP_3R2^{-/-}$ and $IP_3R2^{+/+}$ mice (Fig. 4 *G*–*I* and *SI Appendix*, Table S2), demonstrating that astrocytic cAMP-induced hyperemia is independent of IP_3-mediated Ca^{2+} signaling. The only notable difference was that $IP_3R2^{-/-}$ mice exhibited lower delay of the arteriole dilation response than $IP_3R2^{+/+}$ mice, but similar levels to awake WT mice (Figs. 3*K* and 4*K* and *SI Appendix*, Table S3). Lower cAMP peaks and maximum dilation rate observed in $IP_3R2^{+/+}$ mice compared to WT can be explained by inbreeding-induced variations of transgenic mouse lines and highlight importance of using WT littermates from the same line as internal controls, instead of generic B6 mice (Fig. 4*J*). Although somatic Ca^{2+} is largely diminished in $IP_3R2^{-/-}$ mice, Ca^{2+} signals in astrocytic endfeet are preserved (48) and have been observed concurrently with arteriole dilation (50–52). However, endfeet Ca^{2+} is unlikely to causally contribute to functional hyperemia, as recent in vivo studies using cell type–selective gain-of-function approaches have shown no vasodilation in response to increases in astrocytic Ca^{2+} following optogenetic (19) or pharmacogenetic stimulation of Gq-type GPCR-like constructs (20) in astrocytic soma and processes. Experiments in this study, as well as our previous work (19), were conducted noninvasively via systemic AAV injections and thinned skull preparation in awake conditions. This approach avoids potential confounding factors from ex vivo studies, such as lack of an intact vascular system, and from in vivo studies using cranial windows, which can induce inflammation and reactive gliosis. Additionally, astrocytic Ca^{2+} and cAMP signaling pathways are interconnected in a complex, nonlinear manner (47, 53). Our results show how bPAC-induced elevation of astrocytic cAMP triggers arteriole dilation, followed –after a delay– by an increase in astrocytic Ca^{2+} levels (Fig. 6). We thus provide an alternative possibility that previous studies demonstrating the involvement of astrocytic Ca^{2+} in functional hyperemia could be explained by unobserved increases in cAMP occurring with Ca^{2+} dynamics.

Although several cAMP sensors have been developed recently (54), the physiological dynamics of cAMP in astrocytes have yet to be thoroughly investigated in vivo. Two-photon imaging of cortical astrocytes has shown a ~ 15% increase in Pink Flamindo fluorescence following prolonged noradrenergic axon photostimulation, a ~ 10% increase during fear conditioning foot shocks, and no response to abrupt facial air puff stimulation (24). Additionally, a ~ 60% increase in Pink Flamindo signal was observed in anesthetized mice after topical application of an adenylyl cyclase activator and a phosphodiesterase inhibitor (30). Furthermore, a recent study using the highly sensitive green fluorescence sensor cAMPinG1 reported a ~ 40% signal increase in cortical astrocytes during running (39). In our study, we used one-photon macroscope imaging to assess Pink Flamindo and observed a dose-dependent cAMP increase of 3 to 6% with whisker stimulation under anesthesia (*SI Appendix*, Fig. S1*P*). Startle-induced cAMP response peaked at ~4% and 12% in anesthetized and awake mice, respectively (*SI Appendix*, Fig. S1*N*). bPAC-induced cAMP elevations in cortical astrocytes ranged 55 to 95% (Figs. 1*G*, 3*C*, and 4*B* and *SI Appendix*, Table S1), though low baseline signal may slightly overestimate the true values. These elevations led to arteriole dilation with a 2 to 8-s delay and with peaks at 10 to 15 s, with faster hyperemia occurring in awake states (Figs. 2*J*, 3*K*, and 4*K* and *SI Appendix*, Fig. S2 *D* and *K* and Table S3). We introduced milder bPAC stimulation (1 mW, 25 ms) to elevate the cAMP level by 8%, mimicking sensory-induced settings (Fig. 6*D* and *SI Appendix*, Fig. S1 *N* and *P*). The mild bPAC stimulation led to a ~ 2.2% increase in arteriole diameter, comparable to 2-min whisker stimulation (2.8% dilation; Fig. 6*I* and *SI Appendix*, Fig. S1*Q*). Interestingly, during REM sleep, increases in cerebral blood volume are associated with increased arteriole dilation (55) and increased capillary flow depends on A2a adenosine receptors (56). The vasodilatory effect of adenosine is particularly relevant in epilepsy, as adenosine levels rise during seizures to support the heightened metabolic demands and also contribute to seizure termination by inhibiting neuronal excitability (57). Adenosine, a key regulator of sleep and neuronal activity (58), interacts with astrocytic adenosine receptors (A2a and A2b), which are coupled to adenylyl cyclase (21) via the Gs pathway, influencing brain metabolism and function (25). Adenosine has been shown to be released by presynaptic activity (59) and might be one of the neurotransmitters sensed by astrocytes at the level of neuropil, whose activity was recently shown to be more relevant than neuronal soma activity in inducing hyperemia (60–62). Therefore, it is tempting to speculate that cAMP-induced arteriole dilation may play a role in regulating CBF during sleep/wake transitions and in epilepsy. Our experiments using 0.2-s, 1-s, or 3-s 5 mW LED to induce 55 to 95% elevations in cAMP levels (Figs. 1–4) may better model

conditions involving sustained arteriole dilation driven by tonic astrocytic activation via adenosine, such as during seizure. Conversely, milder bPAC stimulation using 25-ms 1 mW LED, which induces an 8% cAMP increase (Fig. 6), more closely resembles the transient astrocytic signaling underlying sensory-evoked functional hyperemia.

Several molecular mechanisms could explain the vasodilatory effect of astrocytic cAMP. Elevations in astrocytic cAMP elevations can promote glycogenolysis, releasing lactate into the extracellular space, which it is believed to be used by neurons to meet their metabolic needs through the neuron-astrocyte lactate shuttle (8). Once in the extracellular space, astrocytic lactate dissociates almost completely into H^+ ions and lactate anions (63), leading to a decrease in extracellular pH (pH_e). Acidosis is known to enhance CBF by relaxing vascular smooth muscle cells (64). Additionally, elevated extracellular lactate can reduce the clearance of prostaglandin E_2 (PGE_2) by astrocytic transporters, resulting in PGE_2 accumulation, which induces vasodilation (65). Another possibility is that extracellular lactate is taken up by endothelial cells, which highly express endothelial nitric oxide synthase (eNOS), leading to production of nitric oxide, a well-known vasodilator (66–68). Moreover, astrocytic cAMP might promote release into extracellular space of arachidonic acid, whose metabolites PGE_2 and epoxyeicosatrienoic acids are vasoactive (14). Finally, astrocytic cAMP production by adenylyl cyclase reduces ATP reservoir, potentially decreasing Na^+/K^+ ATPase activity and increasing extracellular potassium, which is known to induce artery dilation (69). Further studies are needed to explore these potential mechanisms in greater detail.

In this study, we showed that astrocytic cAMP exerts a causal vasodilatory effect on superficial arterioles, which only minimally regulate blood flow (6) and are resting on the pia mater, directly interacting with the underneath astrocytic endfeet (70). In this study, we use one-photon activation of bPAC instead of two-photon activation (28), thus having less precise spatiotemporal control of cAMP in three dimensions. Our bPAC stimulation presumably affects astrocytes in layers 1 and 2/3 of the cerebral cortex, which are in direct contact with capillaries and penetrating arterioles, major players in functional hyperemia (12). Vasodilatation was shown to propagate from capillaries to upstream arterioles through retrograde electrical signaling in the endothelium (71, 72). This retrograde functional hyperemia theory is further supported by a recent study showing that layer 2/3 vasodynamics correlates better with layer 4 neuronal activity than its own local neuronal activity (73). Thus, we speculate that bPAC-induced dilation of superficial pial arterioles derives from the retrograde propagation of the vascular response from capillaries and penetrating arterioles toward the cortical surface. Further experiments are necessary to extend our findings to penetrating arterioles and capillaries.

Beyond supplying metabolites and oxygen neurons, functional hyperemia may also be essential for brain temperature regulation, neurovascular signaling, vascular network stabilization, and the glymphatic system (4, 74). Here, using advanced optogenetic tools, we showed that astrocytic cAMP elevations causally induce arteriole dilation with a delay of 2 to 8 s and with time-to-peak of 10 to 15 s in both anesthetized and awake mice, independent of IP_3R2-mediated Ca^{2+} signaling. Even low-amplitude cAMP elevations comparable to sensory-evoked levels, effectively triggered arteriole dilation. This finding opens broad avenues for exploring astrocytic cAMP as a mediator of blood flow regulation during natural behaviors, such as sleep, and as a potential therapeutic target for neurological diseases characterized by impaired blood flow, including dementia.

Materials and Methods

Mice. Adult C57BL/6J mice (6 to 7 wk, both sexes) were used in Figs. 1–3, 5, and 6. $IP_3R2^{-/-}$ and $IP_3R2^{+/+}$ littermates (10 to 18 wk, both sexes) were used in Fig. 4: This mouse line is a knock-out for *Itpr2* (inositol 1,4,5-trisphosphate receptor 2) (B6.129S4-Itpr2^{tm1Kmik}, RIKEN BioResource Research Center # RBRC10289) (36). Mice were housed in a 12-h light/12-h dark cycle (lights on: 7 am) with food and water ad libitum. All experiments were approved by the Danish Animal Experiments Inspectorate and were overseen by the University of Copenhagen Institutional Animal Care and Use Committee (IACUC), in compliance with the European Communities Council Directive of 22 September 2010 (2010/63/EU) legislation governing the protection of animals used for scientific purposes.

AAV Injection. For retro-orbital injection, AAV mixture was diluted to 150 µL in sterile saline and administered according to a published protocol (75). Dosage was 2×10^{11} vg for PHP.eB/mGFAP(ABC1D)-2pabPAC(F198Y), AAV8/P3-Alb-mScarlet (2×10^{11} vg), and PHP.eB/hGFAP-GCaMP6f (2×10^{11} vg); 4×10^{11} vg for PHP.eB/mGFAP(ABC1D)-Lck-PinkFlamindo and PHP.eB/hGFAP(ABC1D)-RCaMP3. See *SI Appendix, SI Materials and Methods* for details on AAV preparation.

Thinned Skull and Cranial Window Preparation. Thinned skull preparation was preferred over craniotomy for its less invasive nature, preserving the meninges and avoiding cortical exposure, hence minimizing inflammation and glia activation (19, 40). Mice were kept anesthetized using 1.5% isoflurane on a 37 °C heating pad. Buprenorphine (0.05 mg/kg, s.c.) and lidocaine (0.2 mg/kg, local) were administered for analgesia. After skin excision, a headplate was attached using dental cement (Super Bond C&B, Sun Medical, Shiga, Japan). The skull above the right somatosensory cortex was thinned using a drill to ~40 to 50 µm. Super glue was applied to prevent regrowth and a metal lid was attached with dental silicon to minimize ambient light exposure. The analgesic carprofen (5 mg/kg, s.c.) was given post-op, at 24 h and 48 h. For cranial window preparation for two-photon experiments, skull thinning was replaced by a 4-mm diameter craniotomy sealed with a 4-mm coverslip and dental cement.

In Vivo One-Photon Macroscopic Imaging. Imaging was performed ~3 wk post-AAV injection, with minimum 2 d recovery after skull thinning. Mice were imaged anesthetized (70 mg/kg ketamine, 10 mg/kg xylazine, i.p.) or awake after 3-d head-fixation habituation (20, 40, and 60 min). Fluorescence was examined under a Leica M205 FA macroscope with a X-Cite 200DC light source and a digital camera (C11440 Orca-flash 4.0, Hamamatsu), using ET mCherry filter for Pink Flamindo/Alb-mScarlet and ET-GFP for bPAC. bPAC was activated using a 470 nm blue LED (continuous pulse, 5 mW or 1 mW at the skull level, over a thinned skull area of ~4×4 mm^2) from a Lumencor Spectra X Light Engine. AAV expression was verified with single images (red & green), followed by four ~5 min red-only time-lapse recordings (5 Hz), each consisting of 65 s baseline, LED stimulation (1 s, 0.2 s, 3 s, or 25 ms) and 4 min poststimulation. See *SI Appendix, SI Materials and Methods* for details.

Histology. Deeply anesthetized mice (100 mg/kg ketamine, 20 mg/kg xylazine) were transcardially perfused with sterile saline and then with 4% paraformaldehyde (PFA) in 0.1 M phosphate buffer (pH 7.4) using a peristaltic pump. Brains were postfixed in 4% PFA for 24 h, then stored in PBS. Coronal sections (60 µm) were prepared using a vibratome (Leica VT1200 S) and mounted with antifade mounting medium (Vector laboratories, Vectashield, H-1000) to preserve fluorescence. Images were acquired using an Olympus BX51 Fluorescence Microscope equipped with an Olympus DP74 digital camera. Settings: a 10 × objective lens (Olympus UPlanFL N 10×, NA 0.30), exposure 3 s, gain 0.5×, filter cube U-MGFPHQ (ex BP460-480HQ, em BA495-540HQ) for bPAC and filter cube U-MWIY2 (ex BP545-580, em BA610IF) for Pink Flamindo.

Image Data and Statistical Analysis. All images were preprocessed using Image J and data analysis was done using custom MatLab scripts (Mathworks, USA). See *SI Appendix, SI Materials and Methods* for details.

Values are presented as mean ± SEM. Two-group comparison was assessed by the *t* test, whereas multiple group comparisons, as appropriate: two-sample paired *t* tests with the Benjamini–Hochberg correction for false discovery rate (alpha = 0.05); one-way ANOVA with Tukey's post hoc test; two-way ANOVA; mixed-effects analysis (REML). All statistics were done in Graph Prism 10.

Data, Materials, and Software Availability. All data are uploaded on the DANDI repository (76): https://dandiarchive.org/dandiset/001414. All other data are included in the manuscript and/or *SI Appendix*.

ACKNOWLEDGMENTS. This work was supported by NIH Brain Research Through Advancing Innovative Neurotechnologies Initiative U19 Research Program (U19NS128613, H. Hirase, M.N.), Novo Nordisk Foundation (NNFOC0058058, H. Hirase), Danmarks Frie Forskningsfond (0134-00107B, H. Hirase), Japan Society for the Promotion of Science Grants-in-Aid for Scientific Research (KAKENHI) program (22K06454/24H01221, A.K.; 24K18240, T.Y.; JP23H02782/JP24H00861, M.S.), Japanese Science and Technology Agency ACT-X (JPMJAX211K, T.Y.), Japan Agency for Medical Research and Development (AMED) Brain Mapping by Integrated Neurotechnologies for Disease Studies (Brain/MINDS) (JP21dm0207111, H. Hirai), AMED Brain/MINDS 2.0 (JP24wm0625103, H. Hirai; JP24wm0625119, M.S.), the Lundbeck Foundation (R360-2021-613, R436-2023-1219, H. Hirase), Ono pharmaceutical (H. Hirase), Marie Skłodowska-Curie Fellowship ANCoDy (101064009, A.A.) and Ono pharmaceutical Rising Star Fellowship (A.A.). We thank RIKEN Center for Biosystems Dynamics Research, Kazuko Yahagi (RIKEN Center for Brain Science), Kenji F. Tanaka (Keio University), Tomomi Aida (Tokyo Dental Medical University, Massachusetts Institute of Technology), and Kohichi Tanaka (Tokyo Dental Medical University) for the generation of the Actb$^{em(TRE\text{-}PinkFlamindo)4Hhir}$ mouse. We thank Rafael Yuste and his laboratory (Columbia University) for technical assistance. We thank Dan Xue for helping with the illustration of experimental schemes. We thank Yue Zhao for helping with data upload on the Distributed Archives for Neurophysiology Data Integration repository.

Author affiliations: [a]Center for Translational Neuromedicine, Faculty of Health and Life Sciences, University of Copenhagen, Copenhagen 2200, Denmark; [b]Neurotechnology Center, Department of Biological Sciences, Columbia University, New York, NY 10027; [c]Department of Molecular Medicine - Neurobiology Research, University of Southern Denmark, Odense 5230, Denmark; [d]Department of Neurophysiology and Neural Repair, Gunma University Graduate School of Medicine, Maebashi, Gunma 371-8511, Japan; [e]Viral Vector Core, Initiative for Advanced Research, Gunma University, Maebashi, Gunma 371-8511, Japan; [f]Department of Life Sciences, Graduate School of Arts and Sciences, The University of Tokyo, Meguro, Tokyo 153-8902, Japan; [g]Laboratory for Chemistry and Life Science, Institute of Integrated Research, Institute of Science Tokyo, Yokohama, Kanagawa 226-8501, Japan; [h]Department of Brain Development and Regeneration, Graduate School of Biostudies, Kyoto University, Kyoto 606-8507, Japan; and [i]Center for Translational Neuromedicine, University of Rochester Medical Center, Rochester, NY 14627

1. M. D. Sweeney, K. Kisler, A. Montagne, A. W. Toga, B. V. Zlokovic, The role of brain vasculature in neurodegenerative disorders. *Nat. Neurosci.* **21**, 1318–1331 (2018).
2. K. E. Schlageter, P. Molnar, G. D. Lapin, D. R. Groothuis, Microvessel organization and structure in experimental brain tumors: Microvessel populations with distinctive structural and functional properties. *Microvasc. Res.* **58**, 312–328 (1999).
3. D. Attwell, S. B. Laughlin, An energy budget for signaling in the grey matter of the brain. *J. Cereb. Blood Flow Metab.* **21**, 1133–1145 (2001).
4. P. J. Drew, Neurovascular coupling: Motive unknown. *Trends Neurosci.* **45**, 809–819 (2022).
5. A. R. Nippert, K. R. Biesecker, E. A. Newman, Mechanisms mediating functional hyperemia in the brain. *Neuroscientist* **24**, 73–83 (2018).
6. C. Iadecola, The neurovascular unit coming of age: A journey through neurovascular coupling in health and disease. *Neuron* **96**, 17–42 (2017).
7. A. Verkhratsky, M. Nedergaard, Physiology of astroglia. *Physiol. Rev.* **98**, 239–389 (2018).
8. P. J. Magistretti, I. Allaman, Lactate in the brain: From metabolic end-product to signalling molecule. *Nat. Rev. Neurosci.* **19**, 235–249 (2018).
9. C. A. Durkee, A. Araque, Diversity and specificity of astrocyte–neuron communication. *Neuroscience* **396**, 73–78 (2019).
10. H. Hirase, Y. Iwai, N. Takata, Y. Shinohara, T. Mishima, Volume transmission signalling via astrocytes. *Philos. Trans. R. Soc. Lond. B Biol. Sci.* **369**, 20130604 (2014).
11. P. Kofuji, A. Araque, G-protein-coupled receptors in astrocyte-neuron communication. *Neuroscience* **456**, 71–84 (2021).
12. A. Lia, A. Di Spiezio, M. Speggiorin, M. Zonta, Two decades of astrocytes in neurovascular coupling. *Front. Netw. Physiol.* **3**, 1162757 (2023).
13. M. Nuriya, H. Hirase, "Involvement of astrocytes in neurovascular communication" in *Progress in Brain Research*, K. Masamoto, H. Hirase, K. Yamada, Eds. (Elsevier, 2016), pp. 41–62.
14. A. Mishra, G. R. Gordon, B. A. MacVicar, E. A. Newman, Astrocyte regulation of cerebral blood flow in health and disease. *Cold Spring Harb. Perspect. Biol.* **14**, a041354 (2024)
15. A. Mishra *et al.*, Astrocytes mediate neurovascular signaling to capillary pericytes but not to arterioles. *Nat. Neurosci.* **19**, 1619–1627 (2016).
16. K. Nizar *et al.*, In vivo stimulus-induced vasodilation occurs without IP3 receptor activation and may precede astrocytic calcium increase. *J. Neurosci.* **33**, 8411–8422 (2013).
17. N. Takata *et al.*, Cerebral blood flow modulation by basal forebrain or whisker stimulation can occur independently of large cytosolic Ca^{2+} signaling in astrocytes. *PLoS One* **8**, e66525 (2013).
18. A. P. Del Franco, P. Chiang, E. A. Newman, Dilation of cortical capillaries is not related to astrocyte calcium signaling. *Glia* **70**, 508–521 (2022).
19. K. Ozawa *et al.*, Astrocytic GPCR-induced Ca^{2+} signaling is not causally related to local cerebral blood flow changes. *Int. J. Mol. Sci.* **24**, 13590 (2023).
20. D. E. Bonder, K. D. McCarthy, Astrocytic Gq-GPCR-linked IP3R-dependent Ca^{2+} signaling does not mediate neurovascular coupling in mouse visual cortex *in vivo*. *J. Neurosci.* **34**, 13139–13150 (2014).
21. Z. Zhou, Y. Ikegaya, R. Koyama, The astrocytic cAMP pathway in health and disease. *Int. J. Mol. Sci.* **20**, 779 (2019).
22. V. Gao *et al.*, Astrocytic β_2-adrenergic receptors mediate hippocampal long-term memory consolidation. *Proc. Natl. Acad. Sci. U.S.A.* **113**, 8526–8531 (2016).
23. Z. Zhou *et al.*, Astrocytic cAMP modulates memory via synaptic plasticity. *Proc. Natl. Acad. Sci. U.S.A.* **118**, e2016584118 (2021).
24. Y. Oe *et al.*, Distinct temporal integration of noradrenaline signaling by astrocytic second messengers during vigilance. *Nat. Commun.* **11**, 471 (2020).
25. S. M. Theparambil *et al.*, Adenosine signalling to astrocytes coordinates brain metabolism and function. *Nature* **632**, 139–146 (2024).
26. X. Wang *et al.*, Liver-secreted fluorescent blood plasma markers enable chronic imaging of the microcirculation. *Cell Rep. Methods* **2**, 100302 (2022).
27. M. Vittani *et al.*, "Virally induced CRISPR/Cas9-based knock-in of fluorescent albumin allows long-term visualization of cerebral circulation in infant and adult mice" in *Fluorescence Imaging of the Brain*, D. Rusakov, Ed. (Springer US, 2024), pp. 127–144.
28. T. Kinjo, T. Watabe, K. Kobachi, K. Terai, M. Matsuda, Single-cell activation of the cAMP-signaling pathway in 3D tissues with FRET-assisted two-photon activation of bPAC. *ACS Chem. Biol.* **15**, 2848–2853 (2020).
29. S. Yang *et al.*, PACmn for improved optogenetic control of intracellular cAMP. *BMC Biol.* **19**, 227 (2021).
30. K. Harada *et al.*, Red fluorescent protein-based cAMP indicator applicable to optogenetics and in vivo imaging. *Sci. Rep.* **7**, 7351 (2017).
31. J. Van Unen *et al.*, Kinetics of recruitment and allosteric activation of ARHGEF25 isoforms by the heterotrimeric G-protein Gαq. *Sci. Rep.* **6**, 36825 (2016).
32. A. Rakymzhan, Y. Li, P. Tang, R. K. Wang, Differences in cerebral blood vasculature and flow in awake and anesthetized mouse cortex revealed by quantitative optical coherence tomography angiography. *J. Neurosci. Methods* **353**, 109094 (2021).
33. A. S. Thrane *et al.*, General anesthesia selectively disrupts astrocyte calcium signaling in the awake mouse cortex. *Proc. Natl. Acad. Sci. U.S.A.* **109**, 18974–18979 (2012).
34. M. Stenovec, B. Li, A. Verkhratsky, R. Zorec, Astrocytes in rapid ketamine antidepressant action. *Neuropharmacology* **173**, 108158 (2020).
35. R. L. Rungta, B.-F. Osmanski, D. Boido, M. Tanter, S. Charpak, Light controls cerebral blood flow in naive animals. *Nat. Commun.* **8**, 14191 (2017).
36. A. Futatsugi *et al.*, IP3 receptor types 2 and 3 mediate exocrine secretion underlying energy metabolism. *Science* **309**, 2232–2234 (2005).
37. J. Petravicz, T. A. Fiacco, K. D. McCarthy, Loss of IP_3 receptor-dependent Ca^{2+} increases in hippocampal astrocytes does not affect baseline CA1 pyramidal neuron synaptic activity. *J. Neurosci.* **28**, 4967–4973 (2008).
38. N. Takata *et al.*, Astrocyte calcium signaling transforms cholinergic modulation to cortical plasticity *in vivo*. *J. Neurosci.* **31**, 18155–18165 (2011).
39. T. Yokoyama *et al.*, A multicolor suite for deciphering population coding of calcium and cAMP in vivo. *Nat. Methods* **21**, 897–907 (2024).
40. A. Y. Shih, C. Mateo, P. J. Drew, P. S. Tsai, D. Kleinfeld, A polished and reinforced thinned-skull window for long-term imaging of the mouse brain. *J. Vis. Exp.* **61**, 3742 (2012), 10.3791/3742.
41. P. Gierschik, K. H. Jakobs, "Mechanisms for inhibition of adenylate cyclase by alpha-2 adrenergic receptors" in *The Alpha-2 Adrenergic Receptors*, L. E. Limbird, Ed. (Humana Press, 1988), pp. 75–113.
42. L. Hertz, D. Lovatt, S. A. Goldman, M. Nedergaard, Adrenoceptors in brain: Cellular gene expression and effects on astrocytic metabolism and $[Ca^{2+}]$i. *Neurochem. Int.* **57**, 411–420 (2010).
43. L. P. Munting *et al.*, Spontaneous vasomotion propagates along pial arterioles in the awake mouse brain like stimulus-evoked vascular reactivity. *J. Cereb. Blood Flow Metab.* **43**, 1752–1763 (2023).
44. R. L. Rungta *et al.*, Diversity of neurovascular coupling dynamics along vascular arbors in layer II/III somatosensory cortex. *Commun. Biol.* **4**, 1–11 (2021).
45. M. A. Franceschini *et al.*, The effect of different anesthetics on neurovascular coupling. *Neuroimage* **51**, 1367–1377 (2010).
46. X. Wang *et al.*, Spatiotemporal relationships between neuronal, metabolic, and hemodynamic signals in the awake and anesthetized mouse brain. *Cell Rep.* **43**, 114723 (2024).
47. M. Sobolczyk, T. Boczek, Astrocytic calcium and cAMP in neurodegenerative diseases. *Front. Cell. Neurosci.* **16**, 889939 (2022).
48. R. Srinivasan *et al.*, Ca2+ signaling in astrocytes from IP3R2−/− mice in brain slices and during startle responses in vivo. *Nat. Neurosci.* **18**, 708–717 (2015).
49. M. W. Sherwood, M. Arizono, A. Panatier, K. Mikoshiba, S. H. R. Oliet, Astrocytic IP3rs: Beyond IP3R2. *Front. Cell. Neurosci.* **15**, 695817 (2021).
50. B. L. Lind *et al.*, Fast Ca2+ responses in astrocyte end-feet and neurovascular coupling in mice. *Glia* **66**, 348–358 (2018).
51. G. C. Petzold, D. F. Albeanu, T. F. Sato, V. N. Murthy, Coupling of neural activity to blood flow in olfactory glomeruli is mediated by astrocytic pathways. *Neuron* **58**, 897–910 (2008).
52. A. Krogsgaard *et al.*, PV interneurons evoke astrocytic Ca^{2+} responses in awake mice, which contributes to neurovascular coupling. *Glia* **71**, 1830–1846 (2023).
53. A. Horvat, N. Vardjan, Astroglial cAMP signalling in space and time. *Neurosci. Lett.* **689**, 5–10 (2019).
54. C. I. Massengill, J. Day-Cooney, T. Mao, H. Zhong, Genetically encoded sensors towards imaging cAMP and PKA activity *in vivo*. *J. Neurosci. Methods* **362**, 109298 (2021).
55. K. L. Turner, K. W. Gheres, E. A. Proctor, P. J. Drew, Neurovascular coupling and bilateral connectivity during NREM and REM sleep. *Elife* **9**, e62071 (2020).
56. C.-J. Tsai *et al.*, Cerebral capillary blood flow upsurge during REM sleep is mediated by A2a receptors. *Cell Rep.* **36**, 109558 (2021).
57. L. Weltha, J. Reemmer, D. Boison, The role of adenosine in epilepsy. *Brain Res. Bull.* **151**, 46–54 (2019).
58. T. Porkka-Heiskanen, L. Alanko, A. Kalinchuk, D. Stenberg, Adenosine and sleep. *Sleep Med. Rev.* **6**, 321–332 (2002).

59. Z. Wu *et al.*, Neuronal activity-induced, equilibrative nucleoside transporter-dependent, somatodendritic adenosine release revealed by a GRAB sensor. *Proc. Natl. Acad. Sci. U.S.A.* **120**, e2212387120 (2023).
60. Y.-Y. I. Shih *et al.*, Ultra high-resolution fMRI and electrophysiology of the rat primary somatosensory cortex. *Neuroimage* **73**, 113–120 (2013).
61. C. Mathiesen, K. Caesar, N. Akgören, M. Lauritzen, Modification of activity-dependent increases of cerebral blood flow by excitatory synaptic activity and spikes in rat cerebellar cortex. *J. Physiol.* **512**, 555–566 (1998).
62. N. K. Logothetis, J. Pauls, M. Augath, T. Trinath, A. Oeltermann, Neurophysiological investigation of the basis of the fMRI signal. *Nature* **412**, 150–157 (2001).
63. B. K. Siesjö, "Acid-base homeostasis in the brain: Physiology, chemistry, and neurochemical pathology" in *Molecular Mechanisms of Ischemic Brain Damage*, K. Kogure, K.-A. Hossmann, B. K. Siesjö, F. A. Welsh, Eds. (*Progress in Brain Research*, Elsevier, 1985), vol. **63**, pp. 121–154.
64. C. Aalkjær, H.-L. Peng, pH and smooth muscle. *Acta Physiol. Scand.* **161**, 557–566 (1997).
65. G. R. J. Gordon, H. B. Choi, R. L. Rungta, G. C. R. Ellis-Davies, B. A. MacVicar, Brain metabolism dictates the polarity of astrocyte control over arterioles. *Nature* **456**, 745–749 (2008).
66. N. Tran *et al.*, Endothelial Nitric Oxide Synthase (eNOS) and the cardiovascular system: In physiology and in disease states. *Am. J. Biomed. Sci. Res.* **15**, 153–177 (2022).
67. T. W. Hein, W. Xu, L. Kuo, Dilation of retinal arterioles in response to lactate: Role of nitric oxide, guanylyl cyclase, and ATP-sensitive potassium channels. *Invest. Ophthalmol. Vis. Sci.* **47**, 693–699 (2006).
68. J. J. Montoya, N. Fernández, L. Monge, G. Diéguez, A. L. G. Villalón, Nitric oxide-mediated relaxation to lactate of coronary circulation in the isolated perfused rat heart. *J. Cardiovasc. Pharmacol.* **58**, 392–398 (2011).
69. J. A. Filosa *et al.*, Local potassium signaling couples neuronal activity to vasodilation in the brain. *Nat. Neurosci.* **9**, 1397–1403 (2006).
70. M. S. Thomsen, L. J. Routhe, T. Moos, The vascular basement membrane in the healthy and pathological brain. *J. Cereb. Blood Flow Metab.* **37**, 3300–3317 (2017).
71. T. A. Longden *et al.*, Capillary K^+-sensing initiates retrograde hyperpolarization to locally increase cerebral blood flow. *Nat. Neurosci.* **20**, 717–726 (2017).
72. R. L. Rungta, E. Chaigneau, B.-F. Osmanski, S. Charpak, Vascular compartmentalization of functional hyperemia from the synapse to the pia. *Neuron* **99**, 362–375.e4 (2018).
73. É. Martineau, A. Malescot, N. Elmkinssi, R. L. Rungta, Distal activity patterns shape the spatial specificity of neurovascular coupling. *Nat. Neurosci.* **27**, 2101–2114 (2024).
74. S. Holstein-Rønsbo *et al.*, Glymphatic influx and clearance are accelerated by neurovascular coupling. *Nat. Neurosci.* **26**, 1042–1053 (2023).
75. T. Yardeni, M. Eckhaus, H. D. Morris, M. Huizing, S. Hoogstraten-Miller, Retro-orbital injections in mice. *Lab. Anim.* **40**, 155–160 (2011).
76. M. Vittani *et al.*, Cerebral blood flow is modulated by astrocytic cAMP elevation independently of IP_3R2-mediated Ca^{2+} signaling in mice [Data set]. DANDI Archive. https://doi.org/10.22033/ESGF/CMIP6.7673. Deposited 3 June 2025.